

Adversarial Diffusion Compression for Real-World Image Super-Resolution

Bin Chen^{1,3,*}Gehui Li^{1,*}Rongyuan Wu^{2,3,*}Xindong Zhang³Jie Chen^{1,†}Jian Zhang^{1,†}Lei Zhang^{2,3}¹School of Electronic and Computer Engineering, Peking University²The Hong Kong Polytechnic University³OPPO Research Institute

{chenbin, ligehui921}@stu.pku.edu.cn

rong-yuan.wu@connect.polyu.hk

zhangxindong1@oppo.com

{jiechen2019, zhangjian.sz}@pku.edu.cn

cslzhang@comp.polyu.edu.hk

Abstract

Real-world image super-resolution (Real-ISR) aims to reconstruct high-resolution images from low-resolution inputs degraded by complex, unknown processes. While many Stable Diffusion (SD)-based Real-ISR methods have achieved remarkable success, their slow, multi-step inference hinders practical deployment. Recent SD-based one-step networks like OSEDiff and S3Diff alleviate this issue but still incur high computational costs due to their reliance on large pre-trained SD models. This paper proposes a novel Real-ISR method, **AdcSR**, by distilling the one-step diffusion network OSEDiff into a streamlined diffusion-GAN model under our **Adversarial Diffusion Compression (ADC)** framework. We meticulously examine the modules of OSEDiff, categorizing them into two types: (1) **Removable** (VAE encoder, prompt extractor, text encoder, etc.) and (2) **Prunable** (denoising UNet and VAE decoder). Since direct removal and pruning can degrade the model’s generation capability, we pretrain our pruned VAE decoder to restore its ability to decode images and employ adversarial distillation to compensate for performance loss. This ADC-based diffusion-GAN hybrid design effectively reduces complexity by 73% in inference time, 78% in computation, and 74% in parameters, while preserving the model’s generation capability. Experiments manifest that our proposed AdcSR achieves competitive recovery quality on both synthetic and real-world datasets, offering up to $9.3\times$ speedup over previous one-step diffusion-based methods. Code and models are available at <https://github.com/Guaishou74851/AdcSR>.

1. Introduction

Image super-resolution (ISR) [19, 51, 56, 86, 123] is a fundamental and long-standing problem in computer vision. It aims to reconstruct the high-resolution (HR) image from a low-resolution (LR) counterpart. One line of ISR research assumes that the LR image x_{LR} is a bicubic-downsampled version of the HR image x_{HR} . However, deep ISR networks trained using this assumption often struggle to generalize

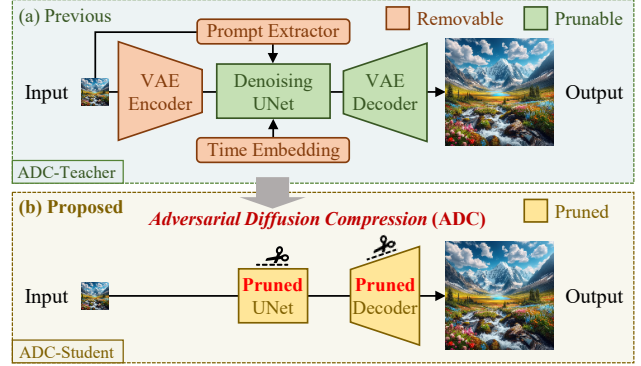


Figure 1. Comparison between our proposed AdcSR and typical one-step diffusion-based Real-ISR methods. (a) The state-of-the-art one-step diffusion network OSEDiff [99] employs complete SD [83] models for Real-ISR, suffering from high computational costs. (b) We distill OSEDiff (ADC-teacher) into a smaller diffusion-GAN hybrid model, **AdcSR** (ADC-student), under the proposed ADC framework, achieving significantly improved efficiency while maintaining competitive recovery performance.

to real-world scenarios, where degradations are more complex and typically unknown. Another increasingly popular line of ISR research, known as real-world ISR (Real-ISR) [93, 117], employs random shufflings of degradation operations and high-order degradation processes to synthesize LR-HR training pairs. These approaches have improved the performance of deep ISR networks in real-world scenarios.

In the field of ISR and Real-ISR, generative adversarial networks (GANs) [4, 24, 27, 52, 64, 92, 108, 125] like SRGAN [44], BSRGAN [117], and Real-ESRGAN [93] have shown greater effectiveness than non-generative models [7–10, 12, 26, 45, 48, 88, 122, 124] in producing realistic details. In addition to GANs, diffusion [13, 17, 38, 80]-based methods such as SR3 [74], StableSR [91], and SeeSR [100] have enhanced the quality of super-resolved images by training powerful diffusion networks [16, 46, 61, 85, 113, 114] and leveraging pretrained text-to-image (T2I) diffusion models [22, 55, 69, 84, 91, 109, 112] such as Stable Diffusion (SD) [68, 73, 78, 83]. However, these GANs and diffusion-based Real-ISR approaches suffer from limited recovery quality or slow inference with tens to hundreds of sampling steps.

Recently, efforts [28, 39, 47, 66, 103] have been made to

This work was supported by OPPO Research Fund.

*Equal Contribution. †Corresponding authors.











Input	SinSR	OSEDiff	S3Diff	AdcSR (Ours)
				
				
Time (s)↓	0.13	0.11	0.28	0.03 (Best)
MACs (G)↓	2649	2265	2621	496 (Best)
#Param. (M)↓	119 (Best)	1775	1327	456

Figure 2. **Comparison of our proposed AdcSR with other existing one-step diffusion-based Real-ISR methods** [94, 99, 115] in terms of visual quality of super-resolution images (top) and model efficiency (bottom). The proposed AdcSR model shows competitive performance in recovering photo-realistic details, while providing the highest inference speed on an NVIDIA A100 GPU, the lowest computational cost, and the second-fewest parameters.

improve the inference speed of diffusion models for Real-ISR. For instance, SinSR [94] distills the 15-step ResShift [114] into a one-step student ISR model. However, it does not utilize large pretrained T2I models and tends to produce oversmoothed results [14, 99, 115]. Building on pretrained SD models, OSEDiff [99] applies variational score distillation (VSD) [97] to ensure the realism of super-resolution images with a one-step diffusion sampling. S3Diff [115] designs a degradation-guided Low-Rank Adaptation (LoRA) [32] module and an online negative sample generation strategy to improve the perceptual quality of images. Nevertheless, the complexity of these approaches in terms of parameter number and inference time can still be too high for real deployments, especially on resource-limited edge devices.

To reduce complexity while maintaining recovery quality, in this paper, we propose a novel diffusion-based Real-ISR model **AdcSR**, which is obtained by applying our proposed adversarial diffusion compression (ADC) framework to OSEDiff. Our main idea is based on the hypothesis that, given LR input \mathbf{x}_{LR} containing abundant information about the target HR image \mathbf{x}_{HR} , a structurally compressed version of SD-based one-step diffusion networks like OSEDiff [99] has a sufficient capacity to learn an effective Real-ISR mapping. As illustrated in Fig. 1, we remove the variational autoencoder (VAE) encoder, prompt extractor, text encoder, cross-attention (CA), and time embedding layers in the SD UNet which we find less important than other modules like self-attention (SA) layers to develop the architecture of AdcSR. Then, we compress the remaining denoising UNet and VAE decoder using channel pruning for improved efficiency. To preserve the model’s generative recovery ability while ensuring training efficiency, inspired by the success of diffusion GANs [34, 37, 54, 60, 76, 77, 96, 101, 105], we pretrain our pruned VAE decoder and introduce adversarial distillation in the feature space of VAE decoder. This enables AdcSR to utilize the information from pretrained SD

and OSEDiff models, as well as the ground truth (GT) images. By doing so, we significantly reduce the complexity of OSEDiff while maintaining competitive recovery quality, as shown in Fig. 2. In summary, our contributions are:

- (1) We introduce ADC, a novel framework that combines structural compression (module removal and pruning) with adversarial distillation (knowledge distillation with adversarial loss) to streamline SD-based one-step Real-ISR models into smaller diffusion-GAN hybrid networks.
- (2) We design a structural compression strategy in ADC: firstly, removing unnecessary modules (VAE encoder, text, and time modules), and then pruning the remaining compressible modules (denoising UNet and VAE decoder).
- (3) We develop a two-stage training scheme in our ADC: firstly, pretraining a channel-pruned VAE decoder, and then distilling one-step teacher into our model with an adversarial loss in the feature space of pretrained VAE decoder.
- (4) By applying ADC to a state-of-the-art SD-based one-step network [99], we propose AdcSR model, a structurally compressed diffusion GAN that effectively achieves a $3.7\times$ inference acceleration and a 74% reduction in parameters.
- (5) Experiments exhibit the competitive Real-ISR performance of our AdcSR model and its appealing efficiency.

2. Related Work

Real-ISR based on LR-HR Pair Synthesis. To make ISR networks applicable to real scenarios, BSRGAN [117] and Real-ESRGAN [93] pioneer the use of shuffled and high-order degradations to synthesize LR-HR pairs for training Real-ISR GANs. They inspire a lot of works [11, 52, 102, 121] that develop new degradation prediction mechanisms [53, 64] and network structures [12, 51]. However, these approaches often suffer from artifacts and oversmoothing.

The success of diffusion models in high-quality generation has prompted researchers to explore leveraging powerful diffusion priors like SD [73, 83] for Real-ISR. Most SD-based methods [55, 84, 112] train adapter modules [65, 119] that use the LR image as control signal to guide the super-resolution processes. For example, StableSR [91] finetunes a time-aware encoder and introduces a controllable feature warping module to balance quality and fidelity. PASD [109] extracts both low-level and high-level features from the LR image and inputs them into the pretrained SD model with a pixel-aware CA module. SeeSR [100] enhances model’s semantic awareness by using degradation-robust tag-style text prompts and soft prompts to guide diffusion sampling. In addition to these, ResShift [114] introduces a new residual shifting-based diffusion model to improve the efficiency of the transition from \mathbf{x}_{LR} to \mathbf{x}_{HR} . However, these approaches require tens to hundreds of iterative steps for diffusion sampling, which increases inference latency and limits their ap-

plication in real deployments where fast inference is critical.

Diffusion Distillation for One-Step Inference. To accelerate the generation process of diffusion models, numerous techniques [25, 29, 58, 58, 63, 72, 75, 104, 106, 127] have been proposed to distill a multi-step diffusion sampling process into a student model with fewer steps. Recent methods [2, 128] further reduce the required number of steps to just one. For instance, InstaFlow [57] distills an ordinary differential equation (ODE) sampling trajectory into a one-step network. Consistency models [59, 81] learn to output consistent results at any timestep. Subsequent works like CTM [37], SDXL-Lightning [54], UFOGen [105], LADD [76, 77], DMD2 [111], and Diffusion2GAN [34] leverage adversarial distillation to improve the quality of generated images using pretrained networks as discriminators. For Real-ISR, SinSR [94] shortens ResShift [114] via bidirectional distillations. OSEDiff [99] introduces VSD [97] approach in latent space to enhance the realism of super-resolved images. Building upon the distilled SD-Turbo [76] models, S3Diff [115] designs a degradation-guided LoRA module and an online negative prompting strategy for improved ISR quality. However, the complexity of existing SD-based one-step diffusion networks remains too high for real deployment on mobile and edge devices due to their large-scale parameters and heavy computation. To mitigate this problem, we structurally compress and distill OSEDiff into a smaller diffusion GAN, enhancing efficiency while maintaining performance.

Structural Compression for Latent Diffusion Models. To achieve photo-realistic image generation, large-scale latent diffusion models [68, 73, 83] are widely employed due to their powerful generative priors. However, the deployment of these models is hindered by their high computation costs. To address this issue, a lot of works [6, 23, 116, 126, 128] have explored compression techniques for efficiency. For example, BK-SDM [36] applies block removal for SD models. SnapFusion [50] designs block-removed UNet and efficient VAE decoder with an improved distillation approach, achieving 8-step T2I inferences. To our knowledge, no existing compression techniques are specifically designed for diffusion-based Real-ISR. In this work, we propose a novel method based on introduced adversarial diffusion compression (ADC). Moving beyond previous one-step approaches [14, 47, 94, 99, 115], we demonstrate that, given LR image as a starting point of super-resolution, the latent encoding, prompt extraction, text-conditioned denoising, and decoding can be compressed into an optimized diffusion GAN.

3. Method

3.1. Preliminary

OSEDiff, and Its Limitations. OSEDiff [99] is a typical state-of-the-art one-step diffusion-based Real-ISR method

that employs a LoRA-finetuned SD VAE encoder $\mathcal{E}_{\text{OSEDiff}}$, a LoRA-finetuned SD UNet $\epsilon_{\text{OSEDiff}}$, a pretrained SD VAE decoder \mathcal{D}_{SD} , and a pretrained prompt extractor \mathcal{C} [100] to perform super-resolution through the following process:

$$\mathbf{z}_{\text{LR}} = \mathcal{E}_{\text{OSEDiff}}(\mathbf{x}_{\text{LR}}), \quad \mathbf{c} = \mathcal{C}(\mathbf{x}_{\text{LR}}), \quad (1)$$

$$\hat{\mathbf{z}}_{\text{HR}} = [\mathbf{z}_{\text{LR}} - \sqrt{1 - \bar{\alpha}_T} \epsilon_{\text{OSEDiff}}(\mathbf{z}_{\text{LR}}; T, \mathbf{c})] / \sqrt{\bar{\alpha}_T}, \quad (2)$$

$$\hat{\mathbf{x}}_{\text{HR}} = \mathcal{D}_{\text{SD}}(\hat{\mathbf{z}}_{\text{HR}}). \quad (3)$$

In Eq. (1), the LR image \mathbf{x}_{LR} is encoded into the VAE latent space, and text prompts \mathbf{c} are extracted from \mathbf{x}_{LR} in parallel. In Eq. (2), one-step diffusion denoising is executed using the noise schedule $\{\bar{\alpha}_t\}$ [31] at the T -th timestep. Finally, in Eq. (3), the denoised latent code is decoded back into image space to obtain the super-resolution image $\hat{\mathbf{x}}_{\text{HR}}$. However, OSEDiff has a total parameter number of 1775M and an inference latency of 0.11s on an NVIDIA A100 GPU for a 512×512 target HR image, which can still be too expensive for real deployment environments where both computational and storage resources are limited. Similar challenges persist in other one-step diffusion-based methods utilizing large-scale pretrained SD models [14, 47, 66, 103, 115].

3.2. Structural Compression Strategy

To improve the efficiency of SD-based Real-ISR methods, we propose an **Adversarial Diffusion Compression (ADC)** framework. Its key insight is that ISR differs from T2I tasks, which rely solely on text inputs for generation, while the LR image in Real-ISR provides rich information about the target HR image. Thus, unlike previous SD-based one-step approaches that employ complete SD model structures, we hypothesize that competitive Real-ISR performance does not require these full architectures, which have been validated to possess sufficient capacity for one-step T2I and Real-ISR (see Sec. 2). Taking OSEDiff [99] as example in this work, we propose that the modules used in Eqs. (1)-(3) contain redundancy and can be removed or pruned for efficiency. To be specific, as shown in Fig. 1, we categorize the modules into two types: (1) **Removable** (VAE encoder, prompt extractor, text encoder, CA layers, and time embeddings) and (2) **Prunable** (denoising UNet and VAE decoder). Based on this categorization, in ADC, we design a structural compression strategy that includes two modifications for SD-based one-step methods: (1) **Removal** of unnecessary modules, and (2) **Pruning** of remaining compressible modules. In the following, we detail and justify these modifications.

3.2.1. Removal of Unnecessary Modules

Eliminating VAE Encoder. In previous SD-based one-step Real-ISR approaches, the VAE encoder maps \mathbf{x}_{LR} to a latent code \mathbf{z}_{LR} , as shown in Eq. (1). This process involves multiple downsampling operations, which can lead to the loss of information important for Real-ISR. To preserve the complete information of the LR input without loss, we eliminate

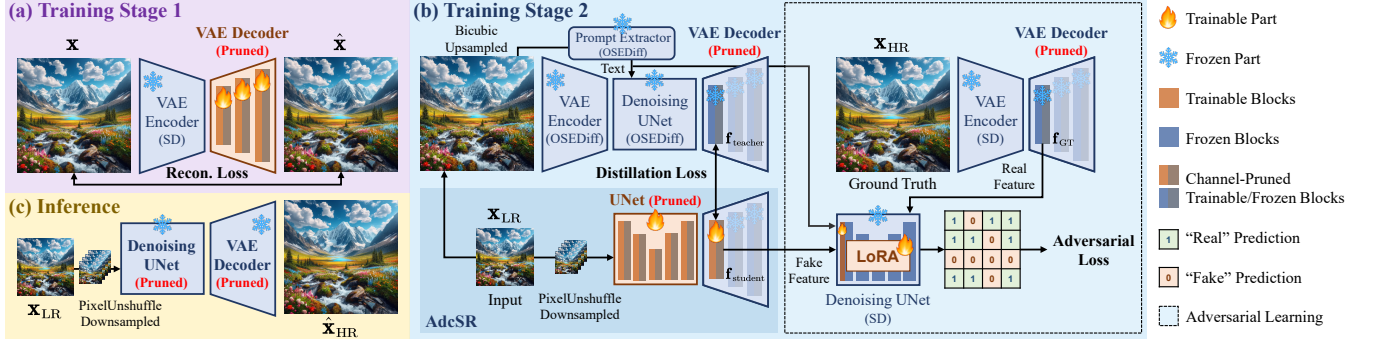


Figure 3. Illustration of the training and inference processes of AdcSR, an instantiation of our ADC framework applied to OSediff. (a) In Stage 1, we pretrain a pruned VAE decoder that shares the latent space with SD and OSediff. (b) In Stage 2, we distill the knowledge from OSediff (ADC-teacher) into AdcSR (ADC-student) by aligning features in the pretrained decoder. An adversarial loss encourages the student to generate features that can fool a LoRA-finetuned SD UNet (ADC-discriminator), utilizing the corresponding real features of GT images. Since all supervisions perform in the feature space, there is no need to decode images as in previous approaches [99, 115]. (c) During inference, the LR image is directly fed into our trained compressed UNet and VAE decoder to obtain the super-resolution result.

the VAE encoder entirely. Instead, we apply a PixelUnshuffle [79] operation to \mathbf{x}_{LR} , rearranging its spatial pixels into channel dimension while maintaining the same spatial size as \mathbf{z}_{LR} . Correspondingly, the first convolution of UNet is adjusted to match the increased channel number, and the output of PixelUnshuffle is then directly input into the UNet.

Removing Text and Time Modules. In models like OSediff, a prompt extractor generates textual prompts from \mathbf{x}_{LR} , which are then used in text encoder and CA layers within the denoising UNet, as shown in Eqs. (1) and (2). Additionally, time embeddings are included to condition the UNet on different timesteps. While the text prompts are generally important for guiding T2I synthesis, in the specific context of Real-ISR, we have empirically observed that they contribute less significantly to enhance quality, compared to the other remaining modules. Furthermore, since OSediff performs only one-step diffusion sampling, time embeddings are unnecessary, as there is no need to differentiate between timesteps. Therefore, we remove the prompt extractor, text encoder, CA layers, and time embeddings from the UNet, retaining only its SA, linear, and convolutional layers.

3.2.2. Pruning of Remaining Modules

Optimizing UNet-VAE Decoder Connection. Before decoding the output image, traditional SD-based methods like OSediff map the high-capacity feature (often hundreds of channels) in UNet to a 4-channel latent code $\hat{\mathbf{z}}_{\text{HR}}$. This dimensionality reduction can potentially result in a loss of feature information and constrain the model’s representation ability. To mitigate this and fully leverage the rich feature representations learned by the UNet, we enhance the information flow between UNet and VAE decoder. Specifically, we remove the output layer of UNet and the input layer of VAE decoder, which reduce and then increase the feature channels. Instead, we introduce a convolution layer that directly connects the high-dimensional feature in UNet to the

first blocks of the VAE decoder, improving the model’s recovery quality while reducing its overall inference latency.

Pruning Feature Channels. We hypothesize that the current one-step model, compressed by the above three operations, still contains redundancy and has sufficient capacity to learn an effective Real-ISR mapping with even fewer parameters. Although previous works [6, 36, 62, 82, 116] compress SD-based models by removing network blocks or layers, we find that this can noticeably degrade the performance of one-step diffusion networks, where the depth of UNet and VAE decoder is already relatively shallow. Further decreasing the depth may impair the ability of model to extract hierarchical features and learn complex transformations for high-quality Real-ISR. To avoid this issue and strike a balance between recovery quality and efficiency, we opt for channel pruning. Concretely, we retain 75% of the feature channels in the UNet and 50% channels in the VAE decoder. This reduces the model’s complexity while alleviating performance loss by preserving network depth.

The resulting structurally compressed model, which we name **AdcSR**, incorporates the proposed two modifications in ADC and consists of three modules: (1) a PixelUnshuffle layer that prepares the LR input image \mathbf{x}_{LR} for processing by rearranging its pixels without information loss; (2) a channel-pruned SD UNet without text encoder, CA layers, and time embeddings, processing the rearranged LR image while keeping the original depth; and (3) a channel-pruned VAE decoder which receives the high-dimensional features from UNet and generates the super-resolution image $\hat{\mathbf{x}}_{\text{HR}}$.

3.3. Training Scheme

Direct removal and pruning can degrade the model’s generative capabilities due to reduced capacity and altered network structure. To mitigate this, as Fig. 3 shows, our ADC uses a two-stage training scheme: (1) pretraining VAE de-

Table 1. **Quantitative comparison of different methods on DRealSR.** Efficiency metrics are tested on an NVIDIA A100 GPU. Throughout this paper, the best, second-best, and third-best results are highlighted in **bold red**, underlined blue, and *italic green*, respectively.

Method	PSNR↑	SSIM↑	LPIPS↓	DISTS↓	NIQE↓	MUSIQ↑	CLIPQA↑	#Steps↓	Time (s)↓	MACs (G)↓	#Param. (M)↓
StableSR [91]	28.03	0.7536	0.3284	0.2269	6.52	58.51	0.6356	200	11.50	79940	1410
DiffBIR [55]	26.71	0.6571	0.4557	0.2748	<i>6.31</i>	61.07	0.6395	50	2.72	24234	1717
SeeSR [100]	<i>28.17</i>	<i>0.7691</i>	0.3189	0.2315	6.40	<u>64.93</u>	0.6804	50	4.30	65857	2524
PASD [109]	27.36	0.7073	0.3760	0.2531	5.55	<i>64.87</i>	0.6808	<i>20</i>	2.80	29125	1900
ResShift [114]	28.46	0.7673	0.4006	0.2656	8.12	50.60	0.5342	<u>15</u>	0.71	5491	119
SinSR [94]	<u>28.36</u>	0.7515	0.3665	0.2485	6.99	55.33	0.6383	1	<i>0.13</i>	2649	119
OSDiff [99]	27.92	0.7835	0.2968	<u>0.2165</u>	6.49	64.65	<i>0.6963</i>	1	<u>0.11</u>	<u>2265</u>	1775
S3Diff [115]	27.39	0.7469	<i>0.3129</i>	0.2108	<i>6.17</i>	64.16	0.7156	1	0.28	<i>2621</i>	<i>1327</i>
AdcSR (Ours)	28.10	<u>0.7726</u>	<u>0.3046</u>	<i>0.2200</i>	6.45	66.26	<u>0.7049</u>	1	0.03	496	<u>456</u>

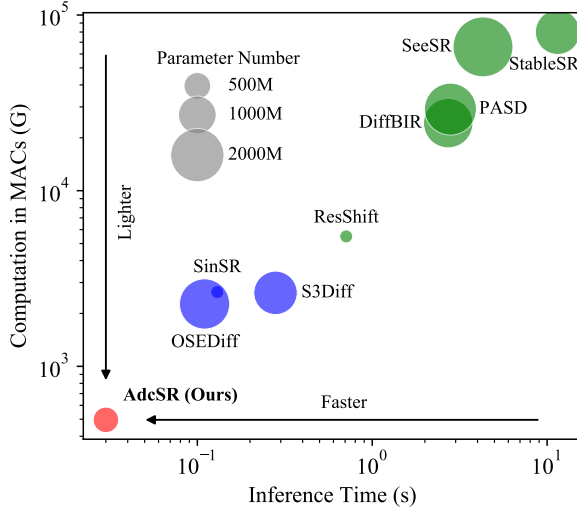


Figure 4. **Efficiency comparison** using a bubble plot, showing the inference time, computation, and parameter number (see Tab. 1) for super-resolving a 128×128 LR image on an NVIDIA A100 GPU. AdcSR achieves the fastest inference, lightest computation, and second-fewest parameters. Bubble colors represent approach types: green for multi-step, blue for one-step, and red for AdcSR.

coder, and (2) adversarial distillation to compensate for potential performance loss and ensure high-quality Real-ISR.

Stage 1: Pretraining Channel-Pruned VAE Decoder. In the first stage, we pretrain a pruned VAE decoder [21, 89] to restore its ability to decode images. As shown in Fig. 3 (a), we freeze the parameters of the pretrained SD VAE encoder and train only the VAE decoder from scratch. Given an input image \mathbf{x} , the encoder produces latent codes, which are then decoded back into an image $\hat{\mathbf{x}}$ by the decoder. To train the decoder, following [73], we adopt a reconstruction loss consisting of a pixel-level L_1 loss $\|\hat{\mathbf{x}} - \mathbf{x}\|_1$, an LPIPS loss [120], and a patch-based adversarial loss [20, 21, 33] to encourage the reconstructed $\hat{\mathbf{x}}$ to be visually similar to \mathbf{x} .

Stage 2: Knowledge Distillation with Adversarial Loss. In the second stage, we distill the knowledge from the pretrained OSDiff (teacher) into our compressed AdcSR (student). Specifically, as illustrated in Fig. 3 (b), we connect the pruned UNet and all the first blocks of pruned decoder at

the level with the smallest spatial size, and jointly finetune them. The student is initialized using the pretrained SD and VAE decoder from Stage 1. Distillation is performed in the feature space by aligning the student’s features $\mathbf{f}_{\text{student}}$ with the teacher’s corresponding features $\mathbf{f}_{\text{teacher}}$ using an L_1 loss:

$$\mathcal{L}_{\text{distill}} = \|\mathbf{f}_{\text{student}} - \mathbf{f}_{\text{teacher}}\|_1. \quad (4)$$

Here, $\mathbf{f}_{\text{teacher}}$ is obtained by passing the LR image through the teacher’s VAE encoder, prompt extractor, UNet, and all first blocks of the pretrained decoder, while $\mathbf{f}_{\text{student}}$ is produced from the student’s pruned UNet and all first blocks of the pruned decoder. This distillation in feature space is both effective and efficient without the need to decode images.

To further enhance the visual quality of super-resolution outputs, we introduce an adversarial loss on $\mathbf{f}_{\text{student}}$, encouraging it to follow the same distribution as the corresponding features of GT images. Specifically, we obtain the real features \mathbf{f}_{GT} by encoding \mathbf{x}_{HR} using SD encoder and processing them with the first blocks of pruned decoder at the smallest spatial size. We reuse a pretrained SD UNet as the discriminator, where the first convolution layer is adjusted to match the channel number of $\mathbf{f}_{\text{student}}$ and \mathbf{f}_{GT} . In addition, we integrate LoRA modules, ensuring that only the LoRA and the first convolution layer remain trainable, while all other parameters are frozen to efficiently finetune the pretrained SD UNet. The discriminator is conditioned on the text prompts \mathbf{c} extracted by the teacher, with timestep fixed at T . Following [110], we employ the non-saturating adversarial loss:

$$\mathcal{L}_{\text{adv}} = \text{Softplus}(-\text{Discriminator}(\mathbf{f}_{\text{student}})), \quad (5)$$

which provides fine-grained feedback as the discriminator’s output shares the same spatial dimension as input features. The total training loss is defined as $\mathcal{L} = \mathcal{L}_{\text{distill}} + \lambda_{\text{adv}}\mathcal{L}_{\text{adv}}$.

4. Experiment

4.1. Experimental Setting

Implementation Details. Following [14, 47, 55, 84, 91, 94, 99, 100, 103, 109, 114, 115], we conduct experiments on the Real-ISR task with scaling factor 4. The sizes of LR and HR

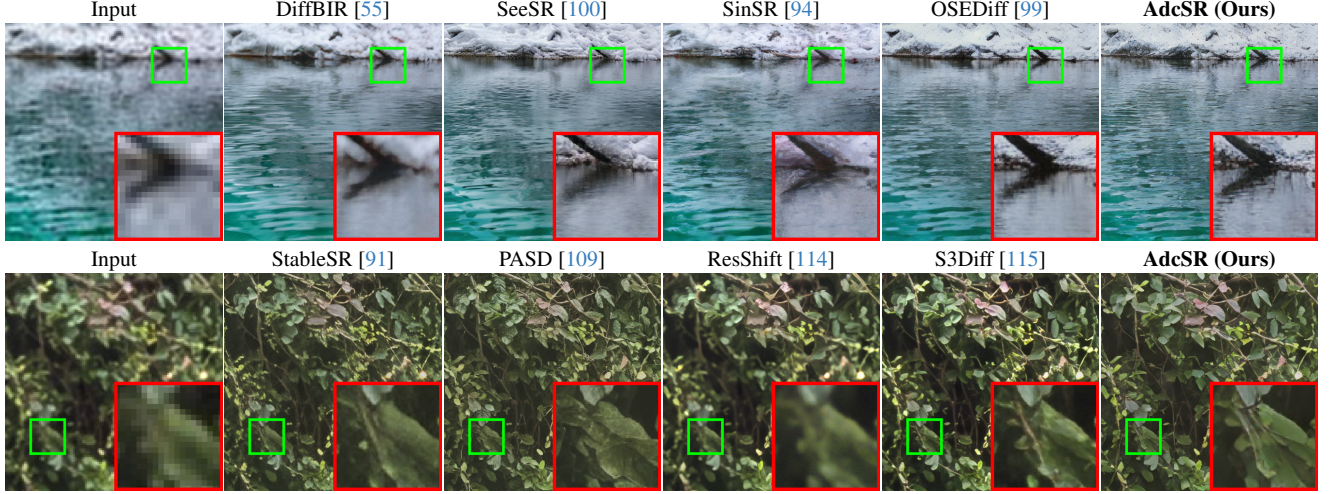


Figure 5. **Qualitative comparison** on images named “0835_pch_00035” from DIV2K-Val (top) and “Nikon_045” from RealSR (bottom).

images are set to 128×128 and 512×512 by default. We initialize our pruned SD UNet using the pretrained weights of SD2.1-base [78], reusing only the parameters corresponding to the first 75% of intermediate feature channels while removing the rest. To match the 64×64 spatial size of latent codes in SD, we set the scaling factor of PixelUnshuffle layer to 2. The convolutional kernels and biases in the first and last UNet layers are repeated in the channel dimension to align with the rearranged LR image and the intermediate features of the first blocks in our pruned SD VAE decoder.

In Stage 1, we employ the code of latent diffusion models [43, 73] to pretrain a 50% channel-pruned SD VAE decoder from scratch on OpenImage [67] for 250K steps, followed by 250K steps on LAION-Face [42] and LAION-Aesthetic [41]. The weighting factors of L_1 loss and LPIPS loss are both set to 1, while the weighting factor of the patch-based adversarial loss is set to 0 for the first 50K steps and 1 for the remaining steps. The learning rate is fixed at $1.3e-6$.

In Stage 2, we jointly finetune the 25% channel-pruned UNet and all first blocks at the smallest spatial size of the pretrained VAE decoder from Stage 1 on LSDIR [49] with $\lambda_{adv} = 1$ for 200K steps. The learning rate is initialized at $1e-4$ and halved for every 100K steps. The learning rate and LoRA rank for the discriminator are set to $1e-6$ and 4, respectively. The high-order degradation pipeline of RealESRGAN [93] is used to synthesize LR-HR pairs. In both two stages, we employ the Adam [40] optimizer and a batch size of 96 for training on 8 NVIDIA A100 (80GB) GPUs.

Test Datasets. Following [99, 100, 115], we test AdcSR and compare it with other methods using the 3K synthesized test images from DIV2K-Val [1, 91] and the center-cropped real images from RealSR [5] and DRealSR [98].

Compared Methods. We compare the proposed AdcSR model against eight diffusion-based approaches: StableSR [91], DiffBIR [55], SeeSR [100], PASD [109], ResShift

[114], SinSR [94], OSDiff [99], and S3Diff [115].

Evaluation Metrics. We adopt both full- and no-reference metrics for performance evaluation. For reference-based fidelity, we use PSNR and SSIM [95], calculated on the Y channel in the YCrCb space. For reference-based perceptual quality, we apply LPIPS [120] and DISTS [18]. FID [30] is also employed to measure the distance between the distributions of GT and super-resolution images. In addition, we utilize no-reference metrics including NIQE [118], MUSIQ [35], MANIQA [107], and CLIPQA [90].

4.2. Comparison with State-of-the-Arts

Recovery Quality Comparison. The first 8 columns of Tab. 1 manifest that our AdcSR achieves promising results across multiple metrics. Firstly, it ranks in top 3 for full-reference quality metrics SSIM, LPIPS, and DISTS, surpassing most other approaches. Secondly, it attains competitive results in PSNR and no-reference metrics NIQE, MUSIQ, and CLIPQA, performing on par with many state-of-the-art methods. Thirdly, compared to the previous one-step diffusion-based models SinSR and particularly its teacher OSDiff, AdcSR yields superiority in most of the perceptual quality metrics, and remains competitive with S3Diff across various cases.

Figs. 2 (top) and 5 exhibit the competitive performance of AdcSR in recovering sharp and photo-realistic images. We observe that StableSR, DiffBIR, SeeSR, and PASD can bring unnatural artifacts and blurriness at the intersection of the rocky landscape and the water, along with noise and distortions in the regions of leaves. ResShift and SinSR suffer from noticeable blurry artifacts. OSDiff and S3Diff could generate fewer details on the surfaces of rocks and water, introducing an additional slight highlight effect on the cluster of leaves. In comparison, AdcSR effectively reconstructs vivid details and natural textures in the regions of parrot’s feathers, building, rocky landscape, still water, and leaves.

Table 2. Ablation study of eliminating VAE encoder on DRealSR.

Method	PSNR \uparrow	LPIPS \downarrow	DISTS \downarrow	#Param. (M) \downarrow	Time (s) \downarrow
w/o Elimination	27.97	0.3077	0.2239	490	0.05
w/ Elim. (Ours)	28.10	0.3046	0.2200	456	0.03

Table 3. Ablation study of optimizing the connection between the denoising UNet and the VAE decoder on DRealSR.

Method	FID \downarrow	MUSIQ \uparrow	MANIQA \uparrow	CLIPQA \uparrow	FPS \uparrow
w/o Optimization	140.09	65.18	0.5807	0.6756	34.66
w/ Opt. (Ours)	134.05	66.26	0.5927	0.7049	34.79

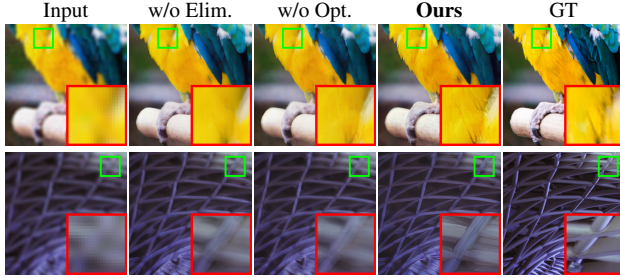


Figure 6. Ablation study of our two structural optimizations: eliminating VAE encoder, and optimizing the connection between the denoising UNet and the VAE decoder on “0886_pch_00025” (top) and “0892_pch_00015” (bottom) from DIV2K-Val.



Figure 7. Ablation study of eliminating VAE encoder on “0815_pch_00001” (left) and “0847_pch_00033” (right) from DIV2K-Val.

Efficiency Comparison. The last 4 columns of Tab. 1 and Fig. 2 (bottom) demonstrate the superior efficiency of proposed AdcSR in step number, inference time, and computational cost. By distilling the SD-based one-step teacher [99] into a structurally compressed diffusion GAN, AdcSR offers substantial speedups: $383.3\times$, $90.7\times$, $143.3\times$, $93.3\times$, and $23.7\times$ over previous multi-step approaches StableSR, DiffBIR, SeeSR, PASD, and ResShift, respectively. Compared to the one-step model SinSR, it achieves a $4.3\times$ acceleration. Compared to its teacher, the previously fastest method OSediff, it achieves a $3.7\times$ acceleration, a 78% reduction in computation, and a 74% decrease in total parameters. This allows for a real-time speed of 34.79 frames per second (FPS) in diffusion-based Real-ISR. Notably, it attains a significant $9.3\times$ speedup over S3Diff, which suffers from slower inferences due to its use of complete SD models and degradation-guided LoRA module. Fig. 4 further visualizes this efficiency comparison using a bubble plot, exhibiting the effective compression and substantial efficiency gains of AdcSR while maintaining recovery quality.

Due to page limitations, please refer to our [Supplementary Material](#) for more comparison results and analyses.

Table 4. Ablation study of removing the prompt extractor, text encoder, time embeddings, and related modules on RealSR.

Method	DISTS \downarrow	#Param. \downarrow	Time \downarrow
w/ Extractor, CA, etc., w/ Time Embeddings	0.2116	1311	0.07
w/o Extractor, CA, etc., w/ Time Embeddings	0.2130	471	0.03
w/o Extr., CA, etc., w/o Time Emb. (Ours)	0.2129	456	0.03

Table 5. Ablation study of pruning feature channels on RealSR.

Pruning Ratio (UNet / VAE Decoder)	LPIPS \downarrow	FID \downarrow	#Param. \downarrow	Time \downarrow
0% / 0% (No Channel Pruning)	0.2883	116.74	839	0.06
0% / 50% (Less Channel Pruning)	0.2839	118.73	801	0.04
25% / 50% (Ours)	0.2885	118.41	456	0.03
50% / 50% (More Channel Pruning)	0.2897	125.10	210	0.03

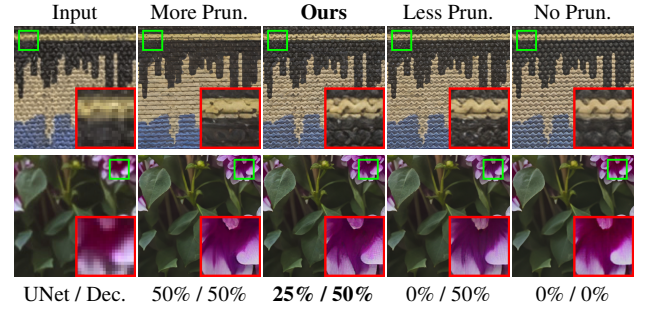


Figure 8. Ablation study of pruning channels with various ratios on “Nikon_027” (top) and “Nikon_043” (bottom) from RealSR.

4.3. Ablation Study

Effect of Eliminating the VAE Encoder, and Optimizing the UNet-VAE Decoder Connection. Tab. 2 exhibits that eliminating the encoder of VAE decreases total parameter number and inference time by 9% and 40%, while achieving improvements of 0.13dB, 0.0031, and 0.0039 in PSNR, LPIPS, and DISTS metrics, respectively. Tab. 3 validates the effectiveness of optimizing the UNet-decoder connection, which brings improvements of 6.04, 1.08, 0.0120, and 0.0293 in FID, MUSIQ, MANIQA, and CLIPQA, as well as a 0.13 FPS gain in the inference speed. Fig. 6 visually demonstrates that omitting either of these two operations leads to noticeable blurriness in the regions of parrot’s body and the intersecting lattice beams. In particular, as exhibited in Fig. 7, using the VAE encoder to compress the LR input into a latent code causes the loss of key characteristics like the clear separation between tree trunks and branches from the background, the details on the left side of the tire, the subtle shadows, and the fine textures on the car headlights. This may be attributed to the information-lossy processing of the VAE encoder. Overall, these findings indicate that directly feeding the LR image into denoising UNet, and connecting the UNet’s features before its final layer to the VAE decoder, without passing through the VAE encoder or compressing into a latent code, can effectively enhance both the fidelity and perceptual quality of super-resolved images.

Table 6. **Ablation study of knowledge distillation** on RealSR.

Method	PSNR \uparrow	NIQE \downarrow	CLIPQA \uparrow
w/o Dist. (Replacing $\mathcal{L}_{\text{distill}}$ with $\ \mathbf{f}_{\text{student}} - \mathbf{f}_{\text{GT}}\ _1$)	26.75	8.59	0.5329
w/ Distillation in Image Space	25.80	6.74	0.4742
w/ Dist. in Feature Space of Level 4	25.54	6.51	0.6168
w/ Dist. in Feature Space of Level 3	25.49	5.91	0.6591
w/ Dist. in Feature Space of Level 2	25.43	5.83	0.6635
w/ Dist. in Feature Space of Level 1 (Ours)	25.47	5.35	0.6731

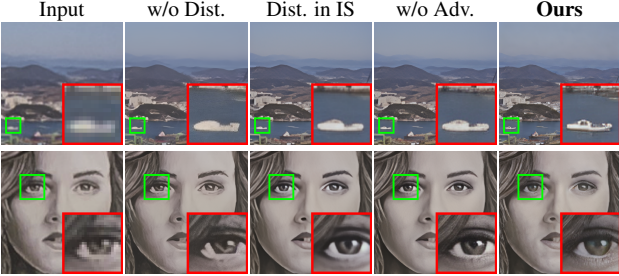


Figure 9. **Ablation study of knowledge distillation in a feature space vs. image space (IS) and the effect of adversarial loss** on “Canon_006” (top) and “Nikon_046” (bottom) from RealSR.

Effect of Removing the Text and Time Modules. Tab. 4 manifests the efficiency gains brought by removing these modules. Concretely, removing extractor, text encoder, and CA layers reduces parameters by 64% and time by 57%, with a 0.0014 increase in DISTS. Furthermore, the removal of time embeddings results in a 0.0001 boost in DISTS and an extra 3% reduction in parameters. Considering the significant decrease in complexity with minor recovery quality drops, these removals are incorporated into our approach.

Effect of Pruning Feature Channels. Tab. 5 presents the results of channel pruning. Our method (pruning 25% channels in the UNet and 50% in the VAE decoder) achieves notable reductions of 46% in parameter number and 50% in inference time compared to the baseline (no channel pruning), with minor drops of 0.0002 in LPIPS and 1.67 in FID. However, more aggressive pruning (50% in both UNet and VAE decoder) leads to a further 54% reduction in parameters but results in a higher increase of 6.69 in FID and no gains in speed. Fig. 8 shows that more pruning significantly impairs the ability of model to recover textures. Therefore, we choose pruning ratios 25% and 50% as default settings.

Effect of Knowledge Distillation in Feature Space. Tab. 6 studies the effect of distilling at various decoder levels, from level 1 (smallest spatial size) to 4 (largest size), and in image space. Firstly, we observe that replacing $\mathbf{f}_{\text{teacher}}$ with \mathbf{f}_{GT} in loss $\mathcal{L}_{\text{distill}} = \|\mathbf{f}_{\text{student}} - \mathbf{f}_{\text{teacher}}\|_1$ significantly degrades the perceptual quality, leading to a deterioration of 3.24 in NIQE and 0.1402 in CLIPQA. This confirms the effectiveness of knowledge distillation. Secondly, conducting distillation in the feature space with smallest spatial size achieves the best perceptual quality, yielding improvements of 1.39

Table 7. **Ablation study of using adversarial loss** on DRealSR.

Method	LPIPS \downarrow	DISTS \downarrow	MUSIQ \uparrow	MANIQA \uparrow
w/o Adversarial Loss	0.3261	0.2392	62.14	0.5650
w/ Adv. (Real Feature: $\mathbf{f}_{\text{teacher}}$)	0.3208	0.2376	66.03	0.5916
w/ Adv. (Real Feat.: \mathbf{f}_{GT}) (Ours)	0.3046	0.2200	66.26	0.5927

in NIQE and 0.1989 in CLIPQA compared to distillation in image space. Fig. 9 visually demonstrates that omitting the distillation or performing it in image domain introduces distortions and blurriness in the super-resolved results, validating the effectiveness of our distillation scheme in ADC.

Effect of Adversarial Loss. Tab. 7 shows the impact of various settings for \mathcal{L}_{adv} . Omitting \mathcal{L}_{adv} significantly degrades perceptual quality by 0.0115, 0.0192, 4.12, and 0.0277 in LPIPS, DISTS, MUSIQ, and CLIPQA, respectively. Using \mathcal{L}_{adv} with real features $\mathbf{f}_{\text{teacher}}$ as in [34] without leveraging \mathbf{f}_{GT} results in non-negligible performance drops of 0.0162, 0.0176, 0.23, and 0.0011 in these four metrics. Fig. 9 further illustrates that, compared to omitting \mathcal{L}_{adv} , our scheme enhances details in the boats and the woman’s face, making textures in the cabin, eyelashes, and iris more natural. These results validate that our adversarial learning scheme effectively utilizes GT to improve the realism of super-resolved images, enabling the model to learn beyond its teacher.

5. Conclusion

In this paper, we proposed a novel method, **AdcSR**, based on our **Adversarial Diffusion Compression (ADC)** framework, for real-world image super-resolution (Real-ISR). To be specific, we structurally compressed a typical state-of-the-art SD-based one-step diffusion network, OSEDiff, into a smaller diffusion GAN. We identified and removed unnecessary modules (VAE encoder, prompt extractor, *etc.*) from OSEDiff, and pruned its remaining compressible modules (denoising UNet and VAE decoder). Since direct removal and pruning can degrade the model’s generative capability, we developed a two-stage training scheme that first pre-trains a pruned SD VAE decoder and then performs adversarial distillation to compensate for performance loss. Experiments on both synthetic and real-world datasets demonstrated that our AdcSR model delivered competitive image quality and superior computational efficiency compared to existing diffusion-based Real-ISR approaches.

While ADC and AdcSR have demonstrated effectiveness in compressing SD-based one-step Real-ISR network and achieving real-time inference, they face challenges in accurately recovering fine textures and heavily degraded details, as shown in Fig. 6. Moreover, although this work focuses on streamlining the state-of-the-art Real-ISR model OSEDiff, our ADC framework could be extended to other SD-based methods. We plan to explore such extensions and integrate additional generative priors for Real-ISR in future work.

Supplementary Material

Our main paper outlines the core idea and techniques of proposed method. It also demonstrates the effectiveness of our four main methodological contributions and adopted settings through experimental validation. In this [Supplementary Material](#), we provide additional details, including the training and inference pseudocode of proposed ADC framework in Sec. A, more ablation studies in Sec. B, more comparison results and a user study analysis in Sec. C, as well as an efficiency evaluation of AdcSR and its SD-based one-step teacher OSEDiff [99] on a real mobile platform, which are not included in the main paper due to space constraints.

A. Pseudocode of Training and Inference

In this section, we present the training and inference procedures of our ADC framework, as summarized in Algo. 1. The training process consists of two stages: (1) pretraining the channel-pruned SD VAE decoder to restore its decoding ability, and (2) knowledge distillation with adversarial loss to compensate for performance degradation due to our compression. The inference of AdcSR is faster than complete SD [73, 83] models due to its compressed structure.

B. More Ablation Studies

Effect of Channel Pruning. Tab. B.1 compares employed channel pruning to other two alternative structural compression strategies: using a block-removed UNet [3, 36] and decoding by the pretrained tiny VAE [15, 87]. We observe that, with similar parameter numbers and inference speed, applying block removal results in a noticeable performance loss of 0.0083 and 0.0084 in LPIPS and DISTS, respectively. While the use of tiny VAE decoder can lead to reductions of 12M parameters and 0.01s in inference time, it substantially degrades performance by 0.0297 and 0.0161 in LPIPS and DISTS. This may be attributed to the reduced depth and the absence of global receptive field in tiny VAE, which relies solely on convolutions for decoding. These results validate the effectiveness of our adopted feature channel pruning.

Effect of Various LoRA Ranks, and Fully Finetuning the First Layer for the Discriminator. Tab. B.2 compares various finetuning settings for discriminator. Fully finetuning it can lead to unstable training without convergence. Compared to the rank of 2, a rank of 4 achieves notable quality gains of 0.0009, 2.09, 6.58, and 0.0139 in evaluation metrics DISTS, FID, MUSIQ, and CLIPQA, respectively. In contrast, higher ranks of 8 and 16 bring no evident improvements. Furthermore, based on the rank of 4, fully finetuning the first convolution layer further enhances performance by 0.0042, 1.26, 1.05, and 0.0536 in these four metrics. These results validate the effectiveness of our default ADC setting.

Table B.1. Ablation study of structural compression on DRealSR.

Method (UNet / VAE Decoder)	LPIPS↓	DISTS↓	#Param.↓	Time↓
Block-Removed / Channel-Pruned	0.3129	0.2284	457	0.03
Channel-Pruned / Tiny VAE Dec.	0.3343	0.2361	444	0.02
Ch.-Pruned / Ch.-Pruned (Ours)	0.3046	0.2200	456	0.03

Table B.2. Ablation study of LoRA rank r and fully finetuning (FT.) the first convolution layer for discriminator on RealSR.

Method	DISTS↓	FID↓	MUSIQ↑	CLIPQA↑
Fully Finetuning the Discriminator	- (No Convergence)			
$r = 2$ (w/o Fully FT. the 1st Layer)	0.2182	121.76	62.27	0.6056
$r = 4$ (w/o Fully FT. the 1st Layer)	0.2171	119.67	68.85	0.6195
$r = 8$ (w/o Fully FT. the 1st Layer)	0.2182	120.94	68.76	0.6114
$r = 16$ (w/o Fully FT. the 1st Layer)	0.2191	120.33	68.72	0.6173
$r = 4$ (w/ Fully FT. 1st Lyr.) (Ours)	0.2129	118.41	69.90	0.6731

C. More Comparison Results on Benchmarks

C.1. More Quantitative Comparisons

In Tab. C.2, we compare the proposed AdcSR model against twelve state-of-the-arts, including four representative GAN-based approaches: BSRGAN [117], Real-ESRGAN [93], LDL [52], and FeMASR [11], as well as eight diffusion-based methods [55, 91, 94, 99, 100, 109, 114, 115] across three synthetic and real-world test datasets, evaluated using nine metrics [18, 30, 35, 90, 95, 107, 118, 120]. We observe that, firstly, the traditional GAN-based approaches generally perform well on reference-based metrics, particularly the fidelity measures PSNR and SSIM. Secondly, diffusion-based methods outperform these GANs in most perceptual quality metrics, showing their ability to better generate natural textures. Thirdly, AdcSR achieves competitive results, surpassing its teacher OSEDiff in most cases, which validates the effectiveness of ADC’s compression and adversarial distillation.

C.2. More Qualitative Comparisons

Figs. C.2, C.3, and C.4 present visual comparisons across super-resolution images produced by these approaches. We observe that, firstly, GAN-based approaches generally show weaker generative capabilities than diffusion-based methods, recovering fewer details overall. Secondly, traditional multi-step SD-based methods generate rich details but may introduce artifacts, such as those observed on the spiky texture of the inflated pufferfish by StableSR, DiffBIR, SeeSR, and PASD. Thirdly, ResShift and SinSR tend to produce oversmoothed results in areas of the leaves and red flower petals, where the vein structures and textures are less distinct. This may be due to their lack of exploiting the powerful SD priors. Fourthly, AdcSR demonstrates competitive performance, generating natural and balanced details in the pufferfish and leaves, comparable to OSEDiff and S3Diff, which can subtly introduce an additional slight highlight effect on the cluster of leaves. These results comprehensively

Algorithm 1: Training and Inference of ADC

Input: Pretrained one-step teacher; Pretrained SD models: VAE encoder \mathcal{E}_{SD} , VAE decoder \mathcal{D}_{SD} , UNet ϵ_{SD} ; Weighting factor λ_{adv} .

Stage 1: Pretraining Pruned VAE Decoder

Prune the SD VAE decoder \mathcal{D}_{SD} to obtain \mathcal{D}_{pruned} ;
Initialize \mathcal{D}_{pruned} and a discriminator as in [43, 73];

for number of training iterations **do**

Sample a batch of images \mathbf{x} ;
Obtain latent codes $\mathbf{z} = \mathcal{E}_{SD}(\mathbf{x})$;
Reconstruct images $\hat{\mathbf{x}} = \mathcal{D}_{pruned}(\mathbf{z})$;
Compute reconstruction loss [73] of \mathbf{x} and $\hat{\mathbf{x}}$;
Update \mathcal{D}_{pruned} using Adam optimizer;
Compute discriminator loss [73] of \mathbf{x} and $\hat{\mathbf{x}}$;
Update discriminator using Adam optimizer;

Stage 2: Adversarial Distillation

Prune the SD UNet ϵ_{SD} to obtain ϵ_{pruned} ;
Initialize the student model using ϵ_{pruned} and \mathcal{D}_{pruned} ;
Initialize a feature-space discriminator using ϵ_{SD} ;

for number of training iterations **do**

Sample a batch of LR-HR pairs $(\mathbf{x}_{LR}, \mathbf{x}_{HR})$;
Compute features $\mathbf{f}_{student}$ from student model;
Compute features $\mathbf{f}_{teacher}$ from teacher model;
Compute distillation loss:

$$\mathcal{L}_{distill} = \|\mathbf{f}_{student} - \mathbf{f}_{teacher}\|_1$$

Compute adversarial loss:

$$\mathcal{L}_{adv} = \text{Softplus}(-\text{Discriminator}(\mathbf{f}_{student}))$$

Compute total loss: $\mathcal{L} = \mathcal{L}_{distill} + \lambda_{adv}\mathcal{L}_{adv}$;
Update student model using Adam optimizer;
Compute features \mathbf{f}_{GT} using \mathbf{x}_{HR} ;
Compute discriminator loss:

$$\mathcal{L}_{disc} = \text{Softplus}(\text{Discriminator}(\mathbf{f}_{student})) \\ + \text{Softplus}(-\text{Discriminator}(\mathbf{f}_{GT}))$$

Update discriminator using Adam optimizer;

Inference;

Given LR image input \mathbf{x}_{LR} ;

return Super-resolved image $\hat{\mathbf{x}}_{HR} = \text{Student}(\mathbf{x}_{LR})$;

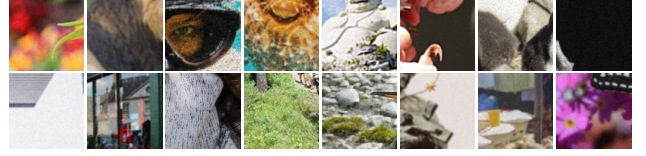


Figure C.1. 16 LR images from DIV2K-Val adopted in user study.

Table C.1. User study results of one-step diffusion-based methods.

Method	SinSR	OSDiff	S3Diff	AdcSR (Ours)
Total Votes	35	149	168	160
Voting Rate (%)	7	29	33	31

C.3. User Study

To further evaluate the effectiveness of our AdcSR, we conduct a user study comparing four one-step diffusion-based Real-ISR methods, including SinSR, OSDiff, S3Diff, and AdcSR. We employ sixteen LR images from the DIV2K-Val dataset, shown in a thumbnail form in Fig. C.1. Thirty-two expert researchers are invited to choose the best super-resolution image for each test sample based on two equally weighted criteria: (1) perceptual quality, focusing on clarity, detail, and realism, and (2) content consistency with the LR input, including alignment in image structure and texture.

As reported in Tab. C.1, AdcSR achieves a high voting rate of 31%, comparable to those of 29% and 33% obtained by OSDiff and S3Diff, both of which employ the complete SD models. Although SinSR has fewer total parameters, its super-resolution quality can be less favorable, as reflected by a lower voting rate of 7%. These results validate that our compressed diffusion-GAN hybrid maintains highly competitive Real-ISR performance while achieving $4.3\times$, $3.7\times$, and $9.3\times$ faster inference than SinSR, OSDiff, and S3Diff, respectively, and reducing computation by 81%, 78%, and 81% in GMACs, thus verifying its appealing efficiency.

D. Efficiency Evaluation on Mobile Device

We conduct an efficiency comparison of the proposed AdcSR method against its teacher model, OSDiff, on a flagship mobile platform, **Qualcomm SM8750 (Snapdragon 8 Gen 4)** [71], utilizing the Hexagon Digital Signal Processor (DSP). All models are evaluated using the Qualcomm AI Engine Direct Software Development Kit (SDK) [70] with 8-bit weights and 16-bit activations (W8A16) quantization for fair comparison. The results reported in Tab. C.3 demonstrate that AdcSR significantly outperforms OSDiff in both speed and resource efficiency. Specifically, AdcSR achieves a $25\times$ acceleration in inference latency, reduces memory footprint by 71% (from 1.7GB to 0.5GB), and decreases storage requirements by 74% (from 1.7GB to 0.4GB). These savings are substantial for practical deployment on mobile devices, where resources are typically con-

confirm the effectiveness of our approach in compressing SD-based models for Real-ISR while maintaining quality.

Table C.2. **Quantitative comparison among thirteen different GAN-based and diffusion-based Real-ISR approaches on both synthetic and real-world benchmarks.** “S” denotes the required number of sampling steps in the diffusion-based method.

Test Dataset	Method	PSNR \uparrow	SSIM \uparrow	LPIPS \downarrow	DISTS \downarrow	FID \downarrow	NIQE \downarrow	MUSIQ \uparrow	MANIQA \uparrow	CLIPQA \uparrow
DIV2K-Val	BSRGAN	24.58	0.6269	0.3351	0.2275	44.23	4.75	61.20	0.5071	0.5247
	Real-ESRGAN	24.29	0.6371	0.3112	0.2141	37.64	4.68	61.06	0.5501	0.5277
	LDL	23.83	0.6344	0.3256	0.2227	42.29	4.86	60.04	0.5350	0.5180
	FeMASR	23.06	0.5887	0.3126	0.2057	35.87	4.74	60.83	0.5074	0.5997
	StableSR-S200	23.26	0.5726	0.3113	0.2048	24.44	4.76	65.92	0.6192	0.6771
	DiffBIR-S50	23.64	0.5647	0.3524	0.2128	30.72	4.70	65.81	0.6210	0.6704
	SeeSR-S50	23.68	0.6043	0.3194	0.1968	25.90	4.81	68.67	0.6240	0.6936
	PASD-S20	23.14	0.5505	0.3571	0.2207	29.20	4.36	68.95	0.6483	0.6788
	ResShift-S15	24.65	0.6181	0.3349	0.2213	36.11	6.82	61.09	0.5454	0.6071
	SinSR-S1	24.41	0.6018	0.3240	0.2066	35.57	6.02	62.82	0.5386	0.6471
	OSDiff-S1	23.72	0.6108	0.2941	0.1976	26.32	4.71	67.97	0.6148	0.6683
	S3Diff-S1	23.52	0.5949	0.2581	0.1725	19.66	4.74	68.01	0.6318	0.7012
	AdcSR-S1 (Ours)	23.74	0.6017	0.2853	0.1899	25.52	4.36	68.00	0.6090	0.6764
DRealSR	BSRGAN	28.75	0.8031	0.2883	0.2142	155.63	6.52	57.14	0.4878	0.4915
	Real-ESRGAN	28.64	0.8053	0.2847	0.2089	147.62	6.69	54.18	0.4907	0.4422
	LDL	28.21	0.8126	0.2815	0.2132	155.53	7.13	53.85	0.4914	0.4310
	FeMASR	26.90	0.7572	0.3169	0.2235	157.78	5.91	53.74	0.4420	0.5464
	StableSR-S200	28.03	0.7536	0.3284	0.2269	148.98	6.52	58.51	0.5601	0.6356
	DiffBIR-S50	26.71	0.6571	0.4557	0.2748	166.79	6.31	61.07	0.5930	0.6395
	SeeSR-S50	28.17	0.7691	0.3189	0.2315	147.39	6.40	64.93	0.6042	0.6804
	PASD-S20	27.36	0.7073	0.3760	0.2531	156.13	5.55	64.87	0.6169	0.6808
	ResShift-S15	28.46	0.7673	0.4006	0.2656	172.26	8.12	50.60	0.4586	0.5342
	SinSR-S1	28.36	0.7515	0.3665	0.2485	170.57	6.99	55.33	0.4884	0.6383
	OSDiff-S1	27.92	0.7835	0.2968	0.2165	135.30	6.49	64.65	0.5899	0.6963
	S3Diff-S1	27.39	0.7469	0.3129	0.2108	119.21	6.17	64.16	0.6081	0.7156
	AdcSR-S1 (Ours)	28.10	0.7726	0.3046	0.2200	134.05	6.45	66.26	0.5927	0.7049
RealSR	BSRGAN	26.39	0.7654	0.2670	0.2121	141.28	5.66	63.21	0.5399	0.5001
	Real-ESRGAN	25.69	0.7616	0.2727	0.2063	135.18	5.83	60.18	0.5487	0.4449
	LDL	25.28	0.7567	0.2766	0.2121	142.71	6.00	60.82	0.5485	0.4477
	FeMASR	25.07	0.7358	0.2942	0.2288	141.05	5.79	58.95	0.4865	0.5270
	StableSR-S200	24.70	0.7085	0.3018	0.2288	128.51	5.91	65.78	0.6221	0.6178
	DiffBIR-S50	24.75	0.6567	0.3636	0.2312	128.99	5.53	64.98	0.6246	0.6463
	SeeSR-S50	25.18	0.7216	0.3009	0.2223	125.55	5.41	69.77	0.6442	0.6612
	PASD-S20	25.21	0.6798	0.3380	0.2260	124.29	5.41	68.75	0.6487	0.6620
	ResShift-S15	26.31	0.7421	0.3460	0.2498	141.71	7.26	58.43	0.5285	0.5444
	SinSR-S1	26.28	0.7347	0.3188	0.2353	135.93	6.29	60.80	0.5385	0.6122
	OSDiff-S1	25.15	0.7341	0.2921	0.2128	123.49	5.65	69.09	0.6326	0.6693
	S3Diff-S1	25.19	0.7315	0.2707	0.1994	110.34	5.33	67.92	0.6398	0.6761
	AdcSR-S1 (Ours)	25.47	0.7301	0.2885	0.2129	118.41	5.35	69.90	0.6360	0.6731

Table C.3. **Efficiency comparison on a flagship mobile device, Qualcomm SM8750 (Snapdragon 8 Gen 4),** for super-resolving an LR input image of size 128×128 with a scaling factor of 4.

Method	Latency (ms) \downarrow	Memory (MB) \downarrow	Storage (MB) \downarrow
OSDiff	1647	1777	1693
AdcSR (Ours)	65	510	435
Reduction Rate (%)	97	71	74

strained. To summarize, AdcSR advances beyond previous SD-based one-step Real-ISR models, providing a more efficient, cost-effective solution for real mobile applications.

References

- [1] Eirikur Agustsson and Radu Timofte. Ntire 2017 challenge on single image super-resolution: Dataset and study. In *Proceedings of the IEEE conference on computer vision and pattern recognition workshops*, pages 126–135, 2017. 6
- [2] David Berthelot, Arnaud Autef, Jierui Lin, Dian Ang Yap, Shuangfei Zhai, Siyuan Hu, Daniel Zheng, Walter Talbott, and Eric Gu. Tract: Denoising diffusion models with transitive closure time-distillation. *arXiv preprint arXiv:2303.04248*, 2023. 3
- [3] BK-SDM-v2-Small. <https://huggingface.co/nota-ai/bk-sdm-v2-small>. 9
- [4] Haoming Cai, Jingwen He, Yu Qiao, and Chao Dong.

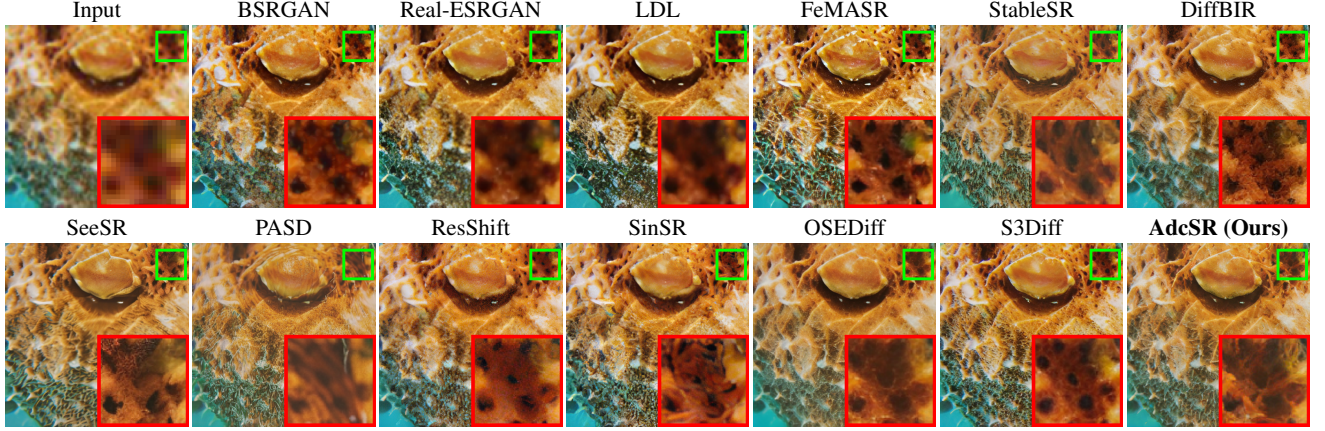


Figure C.2. **Qualitative comparison of different approaches** on an image named “0835_pch_00017” from the DIV2K-Val [91] dataset.

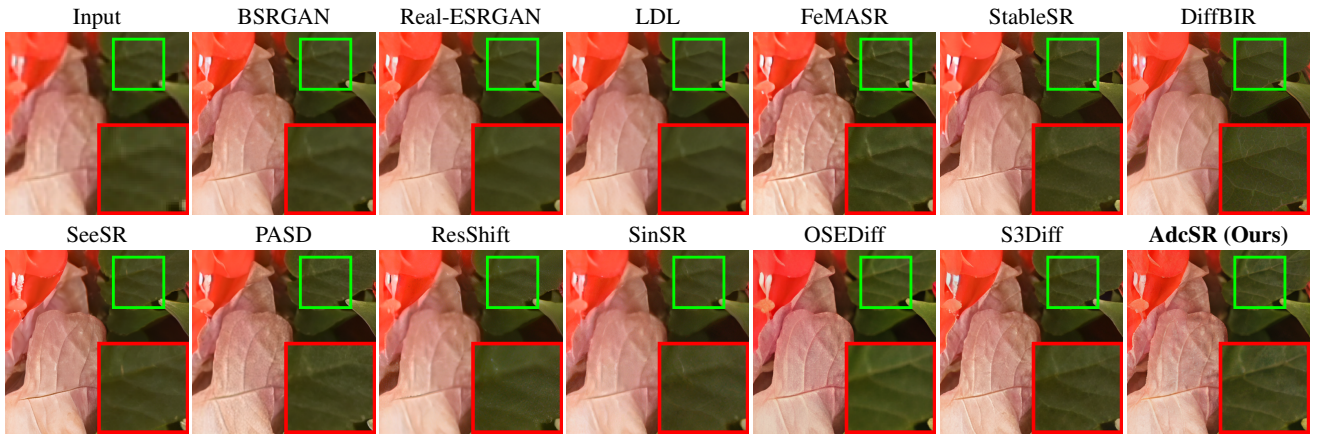


Figure C.3. **Qualitative comparison of different approaches** on a real-world image named “DSC_1599” from the DRealSR [98] dataset.

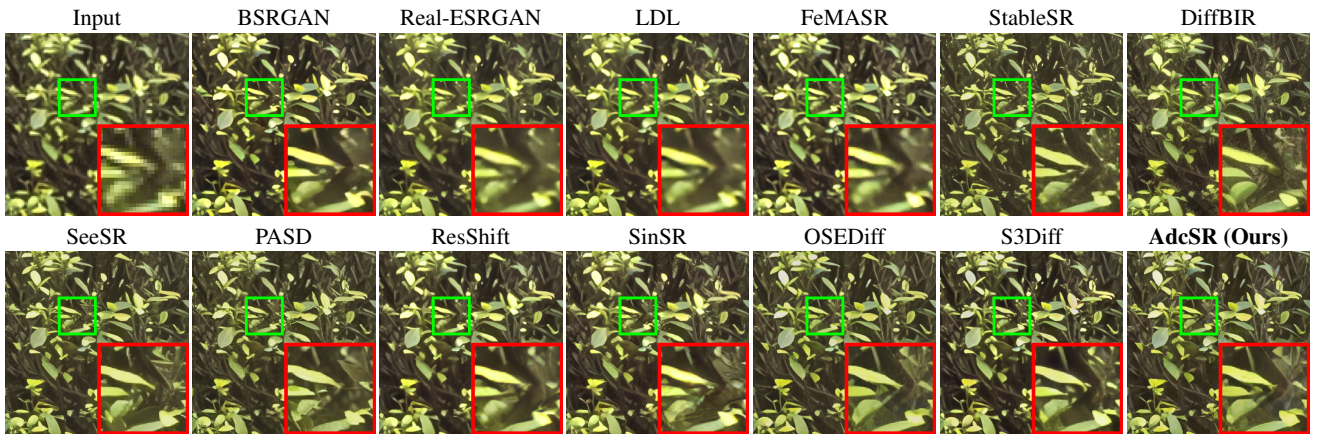


Figure C.4. **Qualitative comparison of different approaches** on a real-world image named “Nikon_013” from the RealSR [5] dataset.

Toward interactive modulation for photo-realistic image restoration. In *Proceedings of the IEEE/CVF Conference on Computer Vision and Pattern Recognition*, pages 294–303, 2021. 1

- [5] Jianrui Cai, Hui Zeng, Hongwei Yong, Zisheng Cao, and Lei Zhang. Toward real-world single image super-

resolution: A new benchmark and a new model. In *Proceedings of the IEEE/CVF international conference on computer vision*, pages 3086–3095, 2019. 6, 12

- [6] Thibault Castells, Hyung-Kyu Song, Tairen Piao, Shinkook Choi, Bo-Kyeong Kim, Hanyoung Yim, Changgun Lee, Jae Gon Kim, and Tae-Ho Kim. Edgefu-

- sion: On-device text-to-image generation. *arXiv preprint arXiv:2404.11925*, 2024. 3, 4
- [7] Bin Chen and Jian Zhang. Content-aware scalable deep compressed sensing. *IEEE Transactions on Image Processing*, 31:5412–5426, 2022. 1
 - [8] Bin Chen and Jian Zhang. Practical compact deep compressed sensing. *IEEE Transactions on Pattern Analysis and Machine Intelligence*, 2024.
 - [9] Bin Chen, Xuanyu Zhang, Shuai Liu, Yongbing Zhang, and Jian Zhang. Self-supervised scalable deep compressed sensing. *International Journal of Computer Vision*, pages 1–36, 2024.
 - [10] Bin Chen, Zhenyu Zhang, Weiqi Li, Chen Zhao, Jiwen Yu, Shijie Zhao, Jie Chen, and Jian Zhang. Invertible diffusion models for compressed sensing. *IEEE Transactions on Pattern Analysis and Machine Intelligence*, 2025. 1
 - [11] Chaofeng Chen, Xinyu Shi, Yipeng Qin, Xiaoming Li, Xiaoguang Han, Tao Yang, and Shihui Guo. Real-world blind super-resolution via feature matching with implicit high-resolution priors. In *Proceedings of the 30th ACM International Conference on Multimedia*, pages 1329–1338, 2022. 2, 9
 - [12] Xiangyu Chen, Xintao Wang, Jiantao Zhou, Yu Qiao, and Chao Dong. Activating more pixels in image super-resolution transformer. In *Proceedings of the IEEE/CVF conference on computer vision and pattern recognition*, pages 22367–22377, 2023. 1, 2
 - [13] Zheng Chen, Haotong Qin, Yong Guo, Xiongfei Su, Xin Yuan, Linghe Kong, and Yulun Zhang. Binarized diffusion model for image super-resolution. *arXiv preprint arXiv:2406.05723*, 2024. 1
 - [14] Qinpeng Cui, Yixuan Liu, Xinyi Zhang, Qiqi Bao, Zhongdao Wang, Qingmin Liao, Li Wang, Tian Lu, and Emad Barsoum. Taming diffusion prior for image super-resolution with domain shift sdes. *arXiv preprint arXiv:2409.17778*, 2024. 2, 3, 5
 - [15] Trung Dao, Thuan Hoang Nguyen, Thanh Le, Duc Vu, Khoi Nguyen, Cuong Pham, and Anh Tran. Swiftbrush v2: Make your one-step diffusion model better than its teacher. In *European Conference on Computer Vision*, pages 176–192. Springer, 2024. 9
 - [16] Mauricio Delbracio and Peyman Milanfar. Inversion by direct iteration: An alternative to denoising diffusion for image restoration. *arXiv preprint arXiv:2303.11435*, 2023. 1
 - [17] Prafulla Dhariwal and Alexander Nichol. Diffusion models beat gans on image synthesis. *Advances in neural information processing systems*, 34:8780–8794, 2021. 1
 - [18] Keyan Ding, Kede Ma, Shiqi Wang, and Eero P Simoncelli. Image quality assessment: Unifying structure and texture similarity. *IEEE transactions on pattern analysis and machine intelligence*, 44(5):2567–2581, 2020. 6, 9
 - [19] Chao Dong, Chen Change Loy, Kaiming He, and Xiaoou Tang. Learning a deep convolutional network for image super-resolution. In *Computer Vision–ECCV 2014: 13th European Conference, Zurich, Switzerland, September 6–12, 2014, Proceedings, Part IV 13*, pages 184–199. Springer, 2014. 1
 - [20] Alexey Dosovitskiy and Thomas Brox. Generating images with perceptual similarity metrics based on deep networks. *Advances in neural information processing systems*, 29, 2016. 5
 - [21] Patrick Esser, Robin Rombach, and Bjorn Ommer. Taming transformers for high-resolution image synthesis. In *Proceedings of the IEEE/CVF conference on computer vision and pattern recognition*, pages 12873–12883, 2021. 5
 - [22] Yuanting Fan, Chengxu Liu, Nengzhong Yin, Changlong Gao, and Xueming Qian. Adadiffsr: Adaptive region-aware dynamic acceleration diffusion model for real-world image super-resolution. 1
 - [23] Gongfan Fang, Xinyin Ma, and Xinchao Wang. Structural pruning for diffusion models. In *Advances in Neural Information Processing Systems*, 2023. 3
 - [24] Ian Goodfellow, Jean Pouget-Abadie, Mehdi Mirza, Bing Xu, David Warde-Farley, Sherjil Ozair, Aaron Courville, and Yoshua Bengio. Generative adversarial nets. *Advances in neural information processing systems*, 27, 2014. 1
 - [25] Jiatao Gu, Shuangfei Zhai, Yizhe Zhang, Lingjie Liu, and Joshua M Susskind. Boot: Data-free distillation of denoising diffusion models with bootstrapping. In *ICML 2023 Workshop on Structured Probabilistic Inference and Generative Modeling*, 2023. 3
 - [26] Jingwen He, Chao Dong, Yihao Liu, and Yu Qiao. Interactive multi-dimension modulation for image restoration. *IEEE Transactions on Pattern Analysis and Machine Intelligence*, 44(12):9363–9379, 2021. 1
 - [27] Jingwen He, Wu Shi, Kai Chen, Lean Fu, and Chao Dong. Gcfsr: a generative and controllable face super resolution method without facial and gan priors. In *Proceedings of the IEEE/CVF conference on computer vision and pattern recognition*, pages 1889–1898, 2022. 1
 - [28] Xiao He, Huao Tang, Zhijun Tu, Junchao Zhang, Kun Cheng, Hanting Chen, Yong Guo, Mingrui Zhu, Nannan Wang, Xinbo Gao, et al. One step diffusion-based super-resolution with time-aware distillation. *arXiv preprint arXiv:2408.07476*, 2024. 1
 - [29] Jonathan Heek, Emiel Hoogeboom, and Tim Salimans. Multistep consistency models. *arXiv preprint arXiv:2403.06807*, 2024. 3
 - [30] Martin Heusel, Hubert Ramsauer, Thomas Unterthiner, Bernhard Nessler, and Sepp Hochreiter. Gans trained by a two time-scale update rule converge to a local nash equilibrium. *Advances in neural information processing systems*, 30, 2017. 6, 9
 - [31] Jonathan Ho, Ajay Jain, and Pieter Abbeel. Denoising diffusion probabilistic models. *Advances in neural information processing systems*, 33:6840–6851, 2020. 3
 - [32] Edward J Hu, Yelong Shen, Phillip Wallis, Zeyuan Allen-Zhu, Yanzhi Li, Shean Wang, Lu Wang, and Weizhu Chen. Lora: Low-rank adaptation of large language models. *arXiv preprint arXiv:2106.09685*, 2021. 2
 - [33] Phillip Isola, Jun-Yan Zhu, Tinghui Zhou, and Alexei A Efros. Image-to-image translation with conditional adversarial networks. In *Proceedings of the IEEE conference on computer vision and pattern recognition*, pages 1125–1134, 2017. 5

- [34] Minguk Kang, Richard Zhang, Connelly Barnes, Sylvain Paris, Suha Kwak, Jaesik Park, Eli Shechtman, Jun-Yan Zhu, and Taesung Park. Distilling diffusion models into conditional gans. *arXiv preprint arXiv:2405.05967*, 2024. 2, 3, 8
- [35] Junjie Ke, Qifei Wang, Yilin Wang, Peyman Milanfar, and Feng Yang. Musiq: Multi-scale image quality transformer. In *Proceedings of the IEEE/CVF international conference on computer vision*, pages 5148–5157, 2021. 6, 9
- [36] Bo-Kyeong Kim, Hyoung-Kyu Song, Thibault Castells, and Shinkook Choi. Bk-sdm: Architecturally compressed stable diffusion for efficient text-to-image generation. In *Workshop on Efficient Systems for Foundation Models@ICML2023*, 2023. 3, 4, 9
- [37] Dongjun Kim, Chieh-Hsin Lai, Wei-Hsiang Liao, Naoki Murata, Yuhta Takida, Toshimitsu Uesaka, Yutong He, Yuki Mitsufuji, and Stefano Ermon. Consistency trajectory models: Learning probability flow ode trajectory of diffusion. *arXiv preprint arXiv:2310.02279*, 2023. 2, 3
- [38] Dongjun Kim, Chieh-Hsin Lai, Wei-Hsiang Liao, Yuhta Takida, Naoki Murata, Toshimitsu Uesaka, Yuki Mitsufuji, and Stefano Ermon. Pagoda: Progressive growing of a one-step generator from a low-resolution diffusion teacher. *arXiv preprint arXiv:2405.14822*, 2024. 1
- [39] Sohwi Kim and Tae-Kyun Kim. Tddsr: Single-step diffusion with two discriminators for super resolution. *arXiv preprint arXiv:2410.07663*, 2024. 1
- [40] Diederik P Kingma. Adam: A method for stochastic optimization. *arXiv preprint arXiv:1412.6980*, 2014. 6
- [41] LAION-Aesthetics. <https://laion.ai/blog/laion-aesthetics/>. 6
- [42] LAION-Face. <https://github.com/FacePerceiver/LAION-Face>. 6
- [43] Latent Diffusion Models. <https://github.com/CompVis/latent-diffusion>. 6, 10
- [44] Christian Ledig, Lucas Theis, Ferenc Huszar, Jose Caballero, Andrew Cunningham, Alejandro Acosta, Andrew Aitken, Alykhan Tejani, Johannes Totz, Zehan Wang, et al. Photo-realistic single image super-resolution using a generative adversarial network. In *Proceedings of the IEEE conference on computer vision and pattern recognition*, pages 4681–4690, 2017. 1
- [45] Gehui Li, Bin Chen, Chen Zhao, Lei Zhang, and Jian Zhang. Osmamba: Omnidirectional spectral mamba with dual-domain prior generator for exposure correction. *arXiv preprint arXiv:2411.15255*, 2024. 1
- [46] Haoying Li, Yifan Yang, Meng Chang, Shiqi Chen, Huajun Feng, Zhihai Xu, Qi Li, and Yueting Chen. Srdiff: Single image super-resolution with diffusion probabilistic models. *Neurocomputing*, 479:47–59, 2022. 1
- [47] Jianze Li, Jiezhong Cao, Zichen Zou, Xiongfei Su, Xin Yuan, Yulun Zhang, Yong Guo, and Xiaokang Yang. Distillation-free one-step diffusion for real-world image super-resolution. *arXiv preprint arXiv:2410.04224*, 2024. 1, 3, 5
- [48] Weiqi Li, Bin Chen, Shuai Liu, Shijie Zhao, Bowen Du, Yongbing Zhang, and Jian Zhang. D3c2-net: Dual-domain deep convolutional coding network for compressive sensing. *IEEE Transactions on Circuits and Systems for Video Technology*, 2024. 1
- [49] Yawei Li, Kai Zhang, Jingyun Liang, Jiezhong Cao, Ce Liu, Rui Gong, Yulun Zhang, Hao Tang, Yun Liu, Denis Demandolx, et al. Lsdrr: A large scale dataset for image restoration. In *Proceedings of the IEEE/CVF Conference on Computer Vision and Pattern Recognition*, pages 1775–1787, 2023. 6
- [50] Yanyu Li, Huan Wang, Qing Jin, Ju Hu, Pavlo Chemerys, Yun Fu, Yanzhi Wang, Sergey Tulyakov, and Jian Ren. Snapfusion: Text-to-image diffusion model on mobile devices within two seconds. *Advances in Neural Information Processing Systems*, 36, 2024. 3
- [51] Jingyun Liang, Jiezhong Cao, Guolei Sun, Kai Zhang, Luc Van Gool, and Radu Timofte. Swinir: Image restoration using swin transformer. In *Proceedings of the IEEE/CVF international conference on computer vision*, pages 1833–1844, 2021. 1, 2
- [52] Jie Liang, Hui Zeng, and Lei Zhang. Details or artifacts: A locally discriminative learning approach to realistic image super-resolution. In *Proceedings of the IEEE/CVF Conference on Computer Vision and Pattern Recognition*, pages 5657–5666, 2022. 1, 2, 9
- [53] Jie Liang, Hui Zeng, and Lei Zhang. Efficient and degradation-adaptive network for real-world image super-resolution. In *European Conference on Computer Vision*, pages 574–591. Springer, 2022. 2
- [54] Shanchuan Lin, Anran Wang, and Xiao Yang. Sdxl-lightning: Progressive adversarial diffusion distillation. *arXiv preprint arXiv:2402.13929*, 2024. 2, 3
- [55] Xinqi Lin, Jingwen He, Ziyan Chen, Zhaoyang Lyu, Bo Dai, Fanghua Yu, Wanli Ouyang, Yu Qiao, and Chao Dong. Diffbir: Towards blind image restoration with generative diffusion prior. *arXiv preprint arXiv:2308.15070*, 2023. 1, 2, 5, 6, 9
- [56] Kai Liu, Haotong Qin, Yong Guo, Xin Yuan, Linghe Kong, Guihai Chen, and Yulun Zhang. 2dquant: Low-bit post-training quantization for image super-resolution. *arXiv preprint arXiv:2406.06649*, 2024. 1
- [57] Xingchao Liu, Xiwen Zhang, Jianzhu Ma, Jian Peng, et al. Instaflo: One step is enough for high-quality diffusion-based text-to-image generation. In *The Twelfth International Conference on Learning Representations*, 2023. 3
- [58] Eric Luhman and Troy Luhman. Knowledge distillation in iterative generative models for improved sampling speed. *arXiv preprint arXiv:2101.02388*, 2021. 3
- [59] Simian Luo, Yiqin Tan, Longbo Huang, Jian Li, and Hang Zhao. Latent consistency models: Synthesizing high-resolution images with few-step inference. *arXiv preprint arXiv:2310.04378*, 2023. 3
- [60] Yihong Luo, Xiaolong Chen, and Jing Tang. You only sample once: Taming one-step text-to-image synthesis by self-cooperative diffusion gans. *arXiv preprint arXiv:2403.12931*, 2024. 2
- [61] Ziwei Luo, Fredrik K Gustafsson, Zheng Zhao, Jens Sjölund, and Thomas B Schön. Image restoration with

- mean-reverting stochastic differential equations. *arXiv preprint arXiv:2301.11699*, 2023. 1
- [62] Xinyin Ma, Gongfan Fang, and Xinchao Wang. Deepcache: Accelerating diffusion models for free. In *Proceedings of the IEEE/CVF Conference on Computer Vision and Pattern Recognition*, pages 15762–15772, 2024. 4
- [63] Chenlin Meng, Robin Rombach, Ruiqi Gao, Diederik Kingma, Stefano Ermon, Jonathan Ho, and Tim Salimans. On distillation of guided diffusion models. In *Proceedings of the IEEE/CVF Conference on Computer Vision and Pattern Recognition*, pages 14297–14306, 2023. 3
- [64] Chong Mou, Xintao Wang, Yanze Wu, Ying Shan, and Jian Zhang. Empowering real-world image super-resolution with flexible interactive modulation. *IEEE Transactions on Pattern Analysis and Machine Intelligence*, 2024. 1, 2
- [65] Chong Mou, Xintao Wang, Liangbin Xie, Yanze Wu, Jian Zhang, Zhongang Qi, and Ying Shan. T2i-adapter: Learning adapters to dig out more controllable ability for text-to-image diffusion models. In *Proceedings of the AAAI Conference on Artificial Intelligence*, pages 4296–4304, 2024. 2
- [66] Mehdi Noroozi, Isma Hadji, Brais Martinez, Adrian Bulat, and Georgios Tzimiropoulos. You only need one step: Fast super-resolution with stable diffusion via scale distillation. *arXiv preprint arXiv:2401.17258*, 2024. 1, 3
- [67] OpenImage. <https://storage.googleapis.com/openimages/web/index.html>. 6
- [68] Dustin Podell, Zion English, Kyle Lacey, Andreas Blattmann, Tim Dockhorn, Jonas Müller, Joe Penna, and Robin Rombach. Sdxl: Improving latent diffusion models for high-resolution image synthesis. *arXiv preprint arXiv:2307.01952*, 2023. 1, 3
- [69] Yunpeng Qu, Kun Yuan, Kai Zhao, Qizhi Xie, Jinhua Hao, Ming Sun, and Chao Zhou. Xpsr: Cross-modal priors for diffusion-based image super-resolution. *arXiv preprint arXiv:2403.05049*, 2024. 1
- [70] Qualcomm AI Engine Direct SDK. <https://www.qualcomm.com/developer/software/qualcomm-ai-engine-direct-sdk>. 10
- [71] Qualcomm Snapdragon Processors. <https://www.qualcomm.com/snapdragon>. 10
- [72] Yuxi Ren, Xin Xia, Yanzuo Lu, Jiacheng Zhang, Jie Wu, Pan Xie, Xing Wang, and Xuefeng Xiao. Hyper-sd: Trajectory segmented consistency model for efficient image synthesis. *arXiv preprint arXiv:2404.13686*, 2024. 3
- [73] Robin Rombach, Andreas Blattmann, Dominik Lorenz, Patrick Esser, and Björn Ommer. High-resolution image synthesis with latent diffusion models. In *Proceedings of the IEEE/CVF conference on computer vision and pattern recognition*, pages 10684–10695, 2022. 1, 2, 3, 5, 6, 9, 10
- [74] Chitwan Saharia, Jonathan Ho, William Chan, Tim Salimans, David J Fleet, and Mohammad Norouzi. Image super-resolution via iterative refinement. *IEEE transactions on pattern analysis and machine intelligence*, 45(4):4713–4726, 2022. 1
- [75] Tim Salimans and Jonathan Ho. Progressive distillation for fast sampling of diffusion models. *arXiv preprint arXiv:2202.00512*, 2022. 3
- [76] Axel Sauer, Dominik Lorenz, Andreas Blattmann, and Robin Rombach. Adversarial diffusion distillation. *arXiv preprint arXiv:2311.17042*, 2023. 2, 3
- [77] Axel Sauer, Frederic Boesel, Tim Dockhorn, Andreas Blattmann, Patrick Esser, and Robin Rombach. Fast high-resolution image synthesis with latent adversarial diffusion distillation. *arXiv preprint arXiv:2403.12015*, 2024. 2, 3
- [78] SD2.1-base. <https://huggingface.co/stabilityai/stable-diffusion-2-1-base>. 1, 6
- [79] Wenzhe Shi, Jose Caballero, Ferenc Huszár, Johannes Totz, Andrew P Aitken, Rob Bishop, Daniel Rueckert, and Zehan Wang. Real-time single image and video super-resolution using an efficient sub-pixel convolutional neural network. In *Proceedings of the IEEE conference on computer vision and pattern recognition*, pages 1874–1883, 2016. 4
- [80] Yang Song, Jascha Sohl-Dickstein, Diederik P Kingma, Abhishek Kumar, Stefano Ermon, and Ben Poole. Score-based generative modeling through stochastic differential equations. *arXiv preprint arXiv:2011.13456*, 2020. 1
- [81] Yang Song, Prafulla Dhariwal, Mark Chen, and Ilya Sutskever. Consistency models. *arXiv preprint arXiv:2303.01469*, 2023. 3
- [82] Yuda Song, Zehao Sun, and Xuanwu Yin. Sdxs: Real-time one-step latent diffusion models with image conditions. *arXiv preprint arXiv:2403.16627*, 2024. 4
- [83] Stability.ai. <https://stability.ai>. 1, 2, 3, 9
- [84] Lingchen Sun, Rongyuan Wu, Zhengqiang Zhang, Hongwei Yong, and Lei Zhang. Improving the stability of diffusion models for content consistent super-resolution. *arXiv preprint arXiv:2401.00877*, 2023. 1, 2, 5
- [85] Qi Tang, Yao Zhao, Meiqin Liu, and Chao Yao. Seeclear: Semantic distillation enhances pixel condensation for video super-resolution. *arXiv preprint arXiv:2410.05799*, 2024. 1
- [86] Radu Timofte, Vincent De Smet, and Luc Van Gool. A+: Adjusted anchored neighborhood regression for fast super-resolution. In *Computer Vision—ACCV 2014: 12th Asian Conference on Computer Vision, Singapore, Singapore, November 1-5, 2014, Revised Selected Papers, Part IV 12*, pages 111–126. Springer, 2015. 1
- [87] Tiny AutoEncoder for Stable Diffusion. <https://huggingface.co/madebyollin/taesd>. 9
- [88] Tong Tong, Gen Li, Xiejie Liu, and Qinquan Gao. Image super-resolution using dense skip connections. In *Proceedings of the IEEE international conference on computer vision*, pages 4799–4807, 2017. 1
- [89] Aaron Van Den Oord, Oriol Vinyals, et al. Neural discrete representation learning. *Advances in neural information processing systems*, 30, 2017. 5
- [90] Jianyi Wang, Kelvin CK Chan, and Chen Change Loy. Exploring clip for assessing the look and feel of images. In *Proceedings of the AAAI Conference on Artificial Intelligence*, pages 2555–2563, 2023. 6, 9
- [91] Jianyi Wang, Zongsheng Yue, Shangchen Zhou, Kelvin CK Chan, and Chen Change Loy. Exploiting diffusion prior for real-world image super-resolution. *International Journal of Computer Vision*, pages 1–21, 2024. 1, 2, 5, 6, 9, 12

- [92] Xintao Wang, Yu Li, Honglun Zhang, and Ying Shan. Towards real-world blind face restoration with generative facial prior. In *Proceedings of the IEEE/CVF conference on computer vision and pattern recognition*, pages 9168–9178, 2021. 1
- [93] Xintao Wang, Liangbin Xie, Chao Dong, and Ying Shan. Real-esrgan: Training real-world blind super-resolution with pure synthetic data. In *Proceedings of the IEEE/CVF international conference on computer vision*, pages 1905–1914, 2021. 1, 2, 6, 9
- [94] Yufei Wang, Wenhan Yang, Xinyuan Chen, Yaohui Wang, Lanqing Guo, Lap-Pui Chau, Ziwei Liu, Yu Qiao, Alex C Kot, and Bihan Wen. Sinsr: diffusion-based image super-resolution in a single step. In *Proceedings of the IEEE/CVF Conference on Computer Vision and Pattern Recognition*, pages 25796–25805, 2024. 2, 3, 5, 6, 9
- [95] Zhou Wang, Alan C Bovik, Hamid R Sheikh, and Eero P Simoncelli. Image quality assessment: from error visibility to structural similarity. *IEEE transactions on image processing*, 13(4):600–612, 2004. 6, 9
- [96] Zhendong Wang, Huangjie Zheng, Pengcheng He, Weizhu Chen, and Mingyuan Zhou. Diffusion-gan: Training gans with diffusion. *arXiv preprint arXiv:2206.02262*, 2022. 2
- [97] Zhengyi Wang, Cheng Lu, Yikai Wang, Fan Bao, Chongxuan Li, Hang Su, and Jun Zhu. Prolificdreamer: High-fidelity and diverse text-to-3d generation with variational score distillation. *Advances in Neural Information Processing Systems*, 36, 2024. 2, 3
- [98] Pengxu Wei, Ziwei Xie, Hannan Lu, Zongyuan Zhan, Qixiang Ye, Wangmeng Zuo, and Liang Lin. Component divide-and-conquer for real-world image super-resolution. In *Computer Vision—ECCV 2020: 16th European Conference, Glasgow, UK, August 23–28, 2020, Proceedings, Part VIII 16*, pages 101–117. Springer, 2020. 6, 12
- [99] Rongyuan Wu, Lingchen Sun, Zhiyuan Ma, and Lei Zhang. One-step effective diffusion network for real-world image super-resolution. *arXiv preprint arXiv:2406.08177*, 2024. 1, 2, 3, 4, 5, 6, 7, 9
- [100] Rongyuan Wu, Tao Yang, Lingchen Sun, Zhengqiang Zhang, Shuai Li, and Lei Zhang. Seesr: Towards semantics-aware real-world image super-resolution. In *Proceedings of the IEEE/CVF conference on computer vision and pattern recognition*, pages 25456–25467, 2024. 1, 2, 3, 5, 6, 9
- [101] Zhisheng Xiao, Karsten Kreis, and Arash Vahdat. Tackling the generative learning trilemma with denoising diffusion gans. *arXiv preprint arXiv:2112.07804*, 2021. 2
- [102] Liangbin Xie, Xintao Wang, Xiangyu Chen, Gen Li, Ying Shan, Jiantao Zhou, and Chao Dong. Desra: detect and delete the artifacts of gan-based real-world super-resolution models. *arXiv preprint arXiv:2307.02457*, 2023. 2
- [103] Rui Xie, Ying Tai, Kai Zhang, Zhenyu Zhang, Jun Zhou, and Jian Yang. Addsr: Accelerating diffusion-based blind super-resolution with adversarial diffusion distillation. *arXiv preprint arXiv:2404.01717*, 2024. 1, 3, 5
- [104] Chen Xu, Tianhui Song, Weixin Feng, Xubin Li, Tiezheng Ge, Bo Zheng, and Limin Wang. Accelerating image generation with sub-path linear approximation model. *arXiv preprint arXiv:2404.13903*, 2024. 3
- [105] Yanwu Xu, Yang Zhao, Zhisheng Xiao, and Tingbo Hou. Ufogen: You forward once large scale text-to-image generation via diffusion gans. In *Proceedings of the IEEE/CVF Conference on Computer Vision and Pattern Recognition*, pages 8196–8206, 2024. 2, 3
- [106] Hanshu Yan, Xingchao Liu, Jiachun Pan, Jun Hao Liew, Qiang Liu, and Jiashi Feng. Perflow: Piecewise rectified flow as universal plug-and-play accelerator. *arXiv preprint arXiv:2405.07510*, 2024. 3
- [107] Sidi Yang, Tianhe Wu, Shuwei Shi, Shanshan Lao, Yuan Gong, Mingdeng Cao, Jiahao Wang, and Yujiu Yang. Maniqa: Multi-dimension attention network for no-reference image quality assessment. In *Proceedings of the IEEE/CVF Conference on Computer Vision and Pattern Recognition*, pages 1191–1200, 2022. 6, 9
- [108] Tao Yang, Peiran Ren, Xuansong Xie, and Lei Zhang. Gan prior embedded network for blind face restoration in the wild. In *Proceedings of the IEEE/CVF conference on computer vision and pattern recognition*, pages 672–681, 2021. 1
- [109] Tao Yang, Rongyuan Wu, Peiran Ren, Xuansong Xie, and Lei Zhang. Pixel-aware stable diffusion for realistic image super-resolution and personalized stylization. *arXiv preprint arXiv:2308.14469*, 2023. 1, 2, 5, 6, 9
- [110] Tianwei Yin, Michaël Gharbi, Taesung Park, Richard Zhang, Eli Shechtman, Fredo Durand, and William T Freeman. Improved distribution matching distillation for fast image synthesis. *arXiv preprint arXiv:2405.14867*, 2024. 5
- [111] Tianwei Yin, Michaël Gharbi, Richard Zhang, Eli Shechtman, Fredo Durand, William T Freeman, and Taesung Park. One-step diffusion with distribution matching distillation. In *Proceedings of the IEEE/CVF Conference on Computer Vision and Pattern Recognition*, pages 6613–6623, 2024. 3
- [112] Fanghua Yu, Jinjin Gu, Zheyuan Li, Jinfan Hu, Xiangtao Kong, Xintao Wang, Jingwen He, Yu Qiao, and Chao Dong. Scaling up to excellence: Practicing model scaling for photo-realistic image restoration in the wild. In *Proceedings of the IEEE/CVF Conference on Computer Vision and Pattern Recognition*, pages 25669–25680, 2024. 1, 2
- [113] Zongsheng Yue, Jianyi Wang, and Chen Change Loy. Efficient diffusion model for image restoration by residual shifting. *arXiv preprint arXiv:2403.07319*, 2024. 1
- [114] Zongsheng Yue, Jianyi Wang, and Chen Change Loy. Resshift: Efficient diffusion model for image super-resolution by residual shifting. *Advances in Neural Information Processing Systems*, 36, 2024. 1, 2, 3, 5, 6, 9
- [115] Aiping Zhang, Zongsheng Yue, Renjing Pei, Wenqi Ren, and Xiaochun Cao. Degradation-guided one-step image super-resolution with diffusion priors. *arXiv preprint arXiv:2409.17058*, 2024. 2, 3, 4, 5, 6, 9
- [116] Dingkun Zhang, Sijia Li, Chen Chen, Qingsong Xie, and Haonan Lu. Laptop-diff: Layer pruning and normalized distillation for compressing diffusion models. *arXiv preprint arXiv:2404.11098*, 2024. 3, 4
- [117] Kai Zhang, Jingyun Liang, Luc Van Gool, and Radu Timofte. Designing a practical degradation model for deep blind image super-resolution. In *Proceedings of the IEEE/CVF*

- International Conference on Computer Vision*, pages 4791–4800, 2021. [1](#), [2](#), [9](#)
- [118] Lin Zhang, Lei Zhang, and Alan C Bovik. A feature-enriched completely blind image quality evaluator. *IEEE Transactions on Image Processing*, 24(8):2579–2591, 2015. [6](#), [9](#)
 - [119] Lvmin Zhang, Anyi Rao, and Maneesh Agrawala. Adding conditional control to text-to-image diffusion models. In *Proceedings of the IEEE/CVF International Conference on Computer Vision*, pages 3836–3847, 2023. [2](#)
 - [120] Richard Zhang, Phillip Isola, Alexei A Efros, Eli Shechtman, and Oliver Wang. The unreasonable effectiveness of deep features as a perceptual metric. In *Proceedings of the IEEE conference on computer vision and pattern recognition*, pages 586–595, 2018. [5](#), [6](#), [9](#)
 - [121] Wenlong Zhang, Xiaohui Li, Guangyuan Shi, Xiangyu Chen, Yu Qiao, Xiaoyun Zhang, Xiao-Ming Wu, and Chao Dong. Real-world image super-resolution as multi-task learning. *Advances in Neural Information Processing Systems*, 36, 2024. [2](#)
 - [122] Xuanyu Zhang, Bin Chen, Wenzhen Zou, Shuai Liu, Yongbing Zhang, Ruiqin Xiong, and Jian Zhang. Progressive content-aware coded hyperspectral snapshot compressive imaging. *IEEE Transactions on Circuits and Systems for Video Technology*, 2024. [1](#)
 - [123] Yulun Zhang, Kunpeng Li, Kai Li, Lichen Wang, Bineng Zhong, and Yun Fu. Image super-resolution using very deep residual channel attention networks. In *Proceedings of the European conference on computer vision (ECCV)*, pages 286–301, 2018. [1](#)
 - [124] Yulun Zhang, Yapeng Tian, Yu Kong, Bineng Zhong, and Yun Fu. Residual dense network for image super-resolution. In *Proceedings of the IEEE conference on computer vision and pattern recognition*, pages 2472–2481, 2018. [1](#)
 - [125] Yuehan Zhang, Seungjun Lee, and Angela Yao. Pairwise distance distillation for unsupervised real-world image super-resolution. *arXiv preprint arXiv:2407.07302*, 2024. [1](#)
 - [126] Yang Zhao, Yanwu Xu, Zhisheng Xiao, and Tingbo Hou. Mobilediffusion: Subsecond text-to-image generation on mobile devices. *arXiv preprint arXiv:2311.16567*, 2023. [3](#)
 - [127] Jianbin Zheng, Minghui Hu, Zhongyi Fan, Chaoyue Wang, Changxing Ding, Dacheng Tao, and Tat-Jen Cham. Trajectory consistency distillation. *arXiv preprint arXiv:2402.19159*, 2024. [3](#)
 - [128] Yuanzhi Zhu, Xingchao Liu, and Qiang Liu. Slimflow: Training smaller one-step diffusion models with rectified flow. In *European Conference on Computer Vision*, pages 342–359. Springer, 2024. [3](#)